JACS
JOURNAL OF THE AMERICAN CHEMICAL SOCIETY
Article
pubs.acs.org/JACS

Single Crystal XRD Structure and Theoretical Analysis of the Chiral $Au_{30}S(S\text{-}t\text{-}Bu)_{18}$ Cluster

David Crasto,[†] Sami Malola,[‡] Grace Brosofsky,[†] Amala Dass,*[,†] and Hannu Häkkinen*[,‡,§]

[†]Department of Chemistry and Biochemistry, University of Mississippi, University, Mississippi 38677, United States
[‡]Department of Physics and [§]Department of Chemistry, Nanoscience Center, University of Jyväskylä, FI-40014 Jyväskylä, Finland

Supporting Information

ABSTRACT: $Au_{30}S(S\text{-}t\text{-}Bu)_{18}$ cluster, related closely to the recently isolated "green gold" compound $Au_{30}(S\text{-}t\text{-}Bu)_{18}$, has been structurally solved via single-crystal XRD and analyzed by density functional theory calculations. The molecular protecting layer shows a combination of monomeric (RS-Au-SR) and trimeric (RS-Au-SR-Au-SR-Au-SR) gold−thiolate units, bridging thiolates, and a single sulfur (sulfide) in a novel μ_3-coordinating position. The chiral gold core has a geometrical component that is identical to the core of the recently reported $Au_{28}(SPh\text{-}t\text{-}Bu)_{20}$. Both enantiomers of $Au_{30}S(S\text{-}t\text{-}Bu)_{18}$ are found in the crystal unit cell. The calculated CD spectrum bears a close resemblance to that of $Au_{28}(SPh\text{-}t\text{-}Bu)_{20}$. This is the first time when two structurally characterized thiol-stabilized gold clusters are found to have such closely related metal core structures and the results may increase understanding of the formation of gold clusters when stabilized by bulky thiolates.

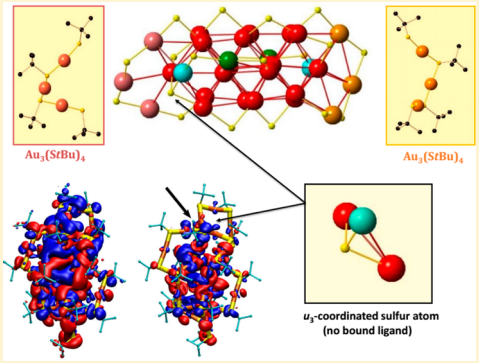

INTRODUCTION

Gold−thiolate clusters $Au_n(SR)_m$ are compounds in the nanometer size regime with a fixed composition that corresponds to a specific number of gold atoms n stabilized by m passivating organic thiolate ligands. These clusters have size-dependent chemical and physical properties. $Au_{25}(SR)_{18}^{-1/0}$, $Au_{38}(SR)_{24}$, and $Au_{144}(SR)_{60}$ are the most commonly studied gold−thiolate clusters,[1a,b] where R = $-SCH_2CH_2Ph$, $-SC_6H_{13}$, $-SC_{12}H_{25}$, all of which are relatively nonbulky ligands. The first-ever crystal structure of $Au_n(SR)_m$ clusters was determined for $Au_{102}(SPhCOOH)_{44}$ in 2007.[1c]

Bulky thiolate ligands are known to modify the packing in self-assembled monolayers (SAMs). Early efforts by Griffin and co-workers[2] working with mixed self-assembled monolayers onto a gold Au(111) substrate revealed less-densely packed monolayer surfaces upon the increase in *tert*-butanethiol concentrations as compared with a straight chain *n*-octadecanethiol. This was attributed to the 5.6 Å van der Waals diameter of the *tert*-butyl group versus that of 4.99 Å between neighboring binding sites on the Au(111) surface. Later efforts by Weiss group[3] using 1-adamantanethiol on SAMs led the researchers to propose a breakdown of the stabilizing van der Waals interactions between neighboring R groups of the ligand that are associated with *n*-alkanethiols.

Employing sterically hindered bulky ligands in nanoparticle synthesis has recently been demonstrated to yield cluster sizes that differ from the commonly observed 25, 38, and 144-atom gold−thiolate clusters. Tracy,[4] Tsukuda,[5] our lab,[6] and others[7] have reported on the uncommon 30, 39, 41, 65-atom Au-SR_{bulky} clusters. Similarly, aromatic thiolate ligands have shown to lead to uncommon altered cluster sizes.[8−10] The effect of aromaticity and bulkiness are coupled intricately when aromatic ligands are employed. Therefore, in the aromatic thiolate cases, it is not possible to attribute the changes in geometric and electronic structure to bulkiness.

Tsukuda[5] first reported the characterization of a monodisperse bulky-ligated $Au_{41}(S\text{-Eind})_{12}$ cluster, after Tracy[4] identified a number of altered-size clusters in a crude mixture of bulky-ligated nanoclusters. Nonetheless, structural information on these uncommon discrete Au-SR clusters, protected by bulky ligands is lacking.

We recently reported the complete isolation of green colored $Au_{30}(S\text{-}t\text{-}Bu)_{18}$, as confirmed by mass spectrometry.[6] Here, we report for the first time the structure of the related $Au_{30}S(St\text{-}Bu)_{18}$ cluster deduced experimentally using X-ray crystallography, and analyze its composition, electronic, optical, and chiroptical properties by using density functional theory (DFT). Our work advances understanding of the effect of bulky ligands on the atomic structure and core geometry of Au-SR clusters.

RESULTS AND DISCUSSION

$Au_{30}(S\text{-}t\text{-}Bu)_{18}$ was synthesized in a one-pot THF method (see Experimental Section for details),[6] and crystallization was performed via vapor−vapor diffusion of ethanol into a toluene solution of $Au_{30}(S\text{-}t\text{-}Bu)_{18}$. Brown colored rhombic-shaped crystals were obtained in 7−10 days. Complete XRD data collection was performed on 7 crystals from different synthetic batches to confirm the unusual structural features.

Received: November 28, 2013
Published: March 7, 2014

   dx.doi.org/10.1021/ja412141j | J. Am. Chem. Soc. 2014, 136, 5000−5005

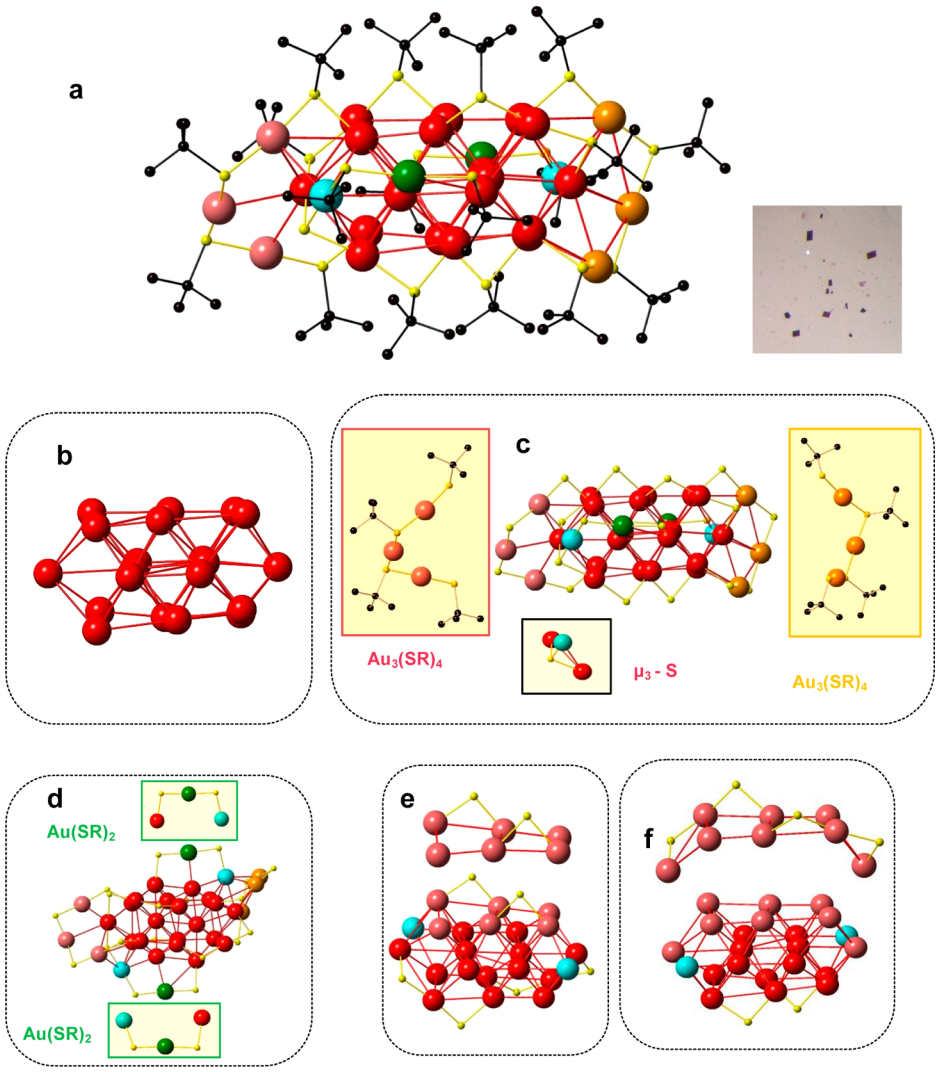

Figure 1. Single crystal XRD structure. (a) Total structure of $Au_{30}S(S\text{-}t\text{-}Bu)_{18}$ (hydrogen atoms are omitted for clarity); (b) Au_{20} interpenetrating bicuboctahedral core geometry; (c) $Au_{30}S_{19}$ geometry showing the triply coordinated μ_3-sulfur and the two trimeric [-SR-Au-SR-Au-SR-Au-SR-] units, highlighted in the orange and pink boxes inset; (d) $Au_{30}S_{19}$ geometry showing the two monomeric [-SR-Au-SR-] units, highlighted in the green box as inset (carbon atoms are omitted in (c) and (d) for clarity); (e and f) the positions of the rest of the SR groups on the Au_{22} bicuboctahedral substructure. The picture inset in (a) shows an optical photograph of the crystals.

Structure. Figure 1a presents the total structure of the $Au_{30}S(St\text{-}Bu)_{18}$ cluster, which crystallizes in a triclinic $P\bar{1}$ space group. The structure was refined to a resolution of 1.12 Å, and to value of 5.90%. By symmetry, most of the Au-atoms are positioned in a Au_{20} bicuboctahedron geometry obeying fcc-symmetry. The geometry, shown in Figure 1b is formed by two interpenetrating Au_{13} atom cuboctahedra, where six of the atoms are shared, as shown previously for Pd_{30} and Au_{28}.[9,11]

Two square faces on the opposite side of the Au_{20} bicuboctahedron are stellated to form a symmetrical Au_{22} substructure of the cluster. The rest of the gold atoms are more separated from the Au_{22} substructure and can be assigned without further analysis as a part of the protecting layer forming two monomeric units [SR-Au-SR] on both sides of the elongated axis of the bicuboctahedron (Figure 1d) and two trimeric units [SR-Au-SR-Au-SR-Au-SR] in both ends of the bicuboctahedron (Figure 1b). The rest of the SR-groups are geometrically in bridge positions and their nature will be analyzed in more detail later. The resolved crystal structure shows remarkably a triply coordinated μ_3-sulfur atom in one end of the bicuboctahedron, totalling to 30 Au atoms and 18 thiolate ligands and one lone-sulfur atom in the cluster. This is the first observation of a μ_3-S in Au-SR molecular systems and has important implications regarding nanoparticle reactivity, as discussed later.

Figure 2A shows the total structure of $Au_{30}S(S\text{-}t\text{-}Bu)_{18}$ cluster along with the analysis of local charges on gold atoms. The structure can be written in the "Divide and Protect" notation[12] as $Au_{30}SL_{18} = Au_{17}@[(Au_3L_4)_2(AuL_2)_2L^b(S\text{-}(Au_2L_2)_2AuL)]$ where L denotes S-*t*-Bu and L^b is a bridging thiolate. This division is based on the Bader DFT analysis of atomic charges on the gold atoms (Figure 2C). A related structure $Au_{30}(S\text{-}t\text{-}Bu)_{18}$, obtained from $Au_{30}S(S\text{-}t\text{-}Bu)_{18}$ by removing the extra sulfur and reoptimizing the cluster via DFT, is shown in Figure 2B. Its composition is $Au_{30}L_{18} = Au_{20}@[(Au_3L_4)_2(AuL_2)_4\ L^b{}_2]$.

The "19th sulfur" in $Au_{30}S(S\text{-}t\text{-}Bu)_{18}$ is in a triply Au-coordinated μ_3 sulfide position, bridging two monomeric AuL_2 units and one bridging SR group into a $S(Au_2L_2)_2AuL$ complex. This structural motif has not previously been encountered in

dx.doi.org/10.1021/ja412141j | J. Am. Chem. Soc. 2014, 136, 5000−5005

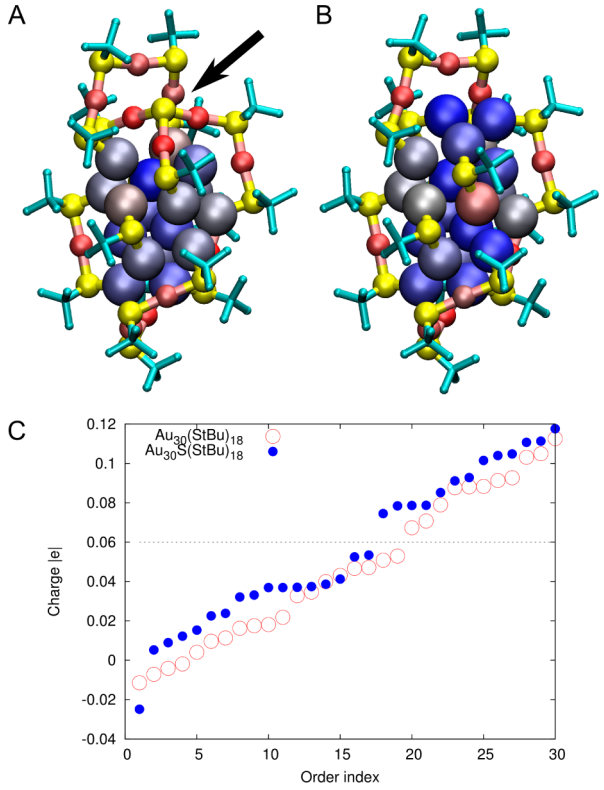

Figure 2. Bader charge analysis on the total structure of $Au_{30}S(S\text{-}t\text{-}Bu)_{18}$ (A) and the DFT-derived structure of $Au_{30}(S\text{-}t\text{-}Bu)_{18}$ (B). The "19th sulfur" is shown by the arrow in (A). Colors of atoms, *t*-Bu blue sticks, sulfur yellow, gold in ranging colors from blue (negative) to red (positive) according to the DFT charge analysis as follows: (A) from −0.025|e| to +0.118|e|, (B) from −0.012|e| to +0.113|e|. The "19th sulfur" in (A) has the charge of −0.32|e|. Both clusters have a clockwise chiral core shown also in Figure 3. (C) Charges of Au-atoms ordered from the lowest to the highest. A stepwise change in the charge of the atoms is shown as a dashed line. When compared to (A) and (B), all the reddish atoms are shown above the line and all the gray and blue atoms are below the line.

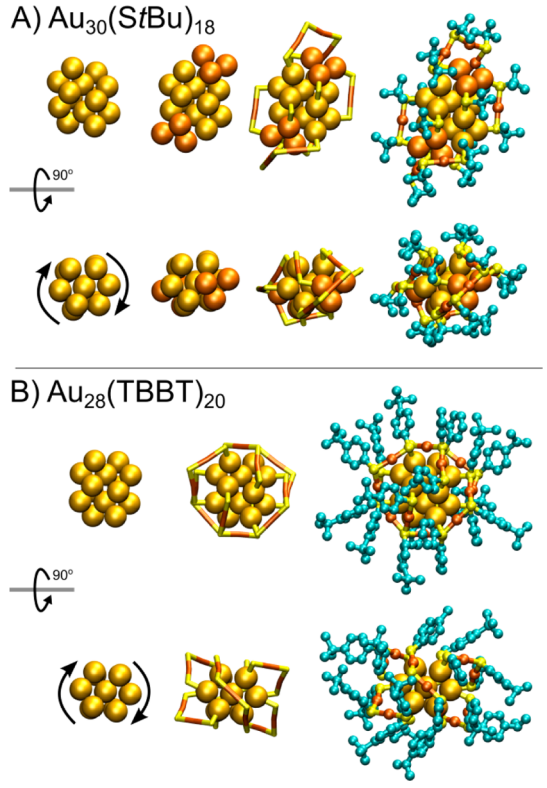

Figure 3. Comparison of the structures of (A) $Au_{30}(S\text{-}t\text{-}Bu)_{18}$ and (B) $Au_{28}(SPh\text{-}t\text{-}Bu)_{20}$[9,14] clusters. Two orthogonal views on the structure are shown for both clusters. The Au_{14} chiral (here the clockwise enantiomer is shown) core of $Au_{28}(SPh\text{-}t\text{-}Bu)_{20}$ in (B, left) forms also the nucleus of $Au_{30}(S\text{-}t\text{-}Bu)_{18}$ (A, left). On top of that nucleus, the Au_{20} core of $Au_{30}(S\text{-}tBu)_{18}$ features two Au_3 triangles on both ends of the core (the orange spheres in (A)).

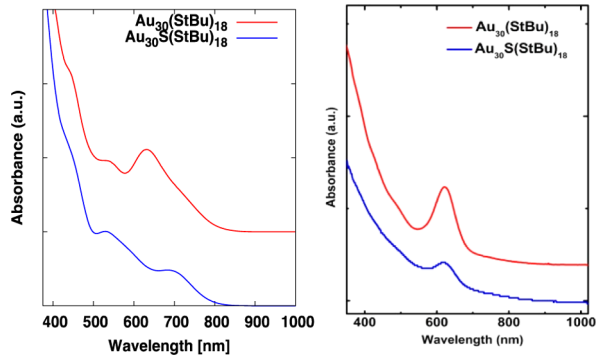

Figure 4. (Left) Calculated and (right) experimental optical absorption spectra of $Au_{30}S(S\text{-}t\text{-}Bu)_{18}$ and $Au_{30}(S\text{-}t\text{-}Bu)_{18}$. The only clearly distinguishable feature between the two different clusters is the peak at 630 nm. Note that the blue curve in (b) is measured from a sample that still contains trace amounts of $Au_{30}(S\text{-}t\text{-}Bu)_{18}$.

thiolate-stabilized Au:SR clusters. However, μ_3-S is known from previous work on sulfide-bridged Au−Ag clusters.[13]

Figure 3 unveils a remarkable similarity in the metal core structure of $Au_{30}(S\text{-}t\text{-}Bu)_{18}$ to the previously reported $Au_{28}(SPh\text{-}t\text{-}Bu)_{20}$ (ref 9). Specifically, the Au_{14} core of $Au_{28}(SPh\text{-}t\text{-}Bu)_{20}$ (ref 14) forms the nucleus of the Au_{20} core of $Au_{30}(S\text{-}t\text{-}Bu)_{18}$. Both cores are chiral. Orientation of the gold−thiolate units also partly resembles each other as the bridged SR-groups are, for example, part of the long trimeric $Au_3(SR)_4$ units in Au_{28} cluster together with one of the monomeric units. Moreover, the position of the extra sulfur atom in the end of the core of $Au_{30}S(S\text{-}t\text{-}Bu)_{18}$ cluster is in close connection to the trimeric unit arrangement in Au_{28} cluster.

Analysis of the Optical and Chiroptical Properties. Optical absorption calculations clearly show that the only feature that sets $Au_{30}(S\text{-}t\text{-}Bu)_{18}$ apart from $Au_{30}S(S\text{-}t\text{-}Bu)_{18}$ is the peak at 630 nm (Figure 4). The computed HOMO−LUMO gaps are 1.45 and 1.37 eV for $Au_{30}(S\text{-}t\text{-}Bu)_{18}$ and $Au_{30}S(S\text{-}t\text{-}Bu)_{18}$, respectively. The electronic states contributing to the 630 nm peak and the induced densities are shown in Figure 5 for both clusters, using an analysis method developed by some of us recently.[15] The strongest contribution to the 630 nm peak comes from the transitions from HOMO−2 state to degenerate HOMO+1 and HOMO+2 states in $Au_{30}(S\text{-}t\text{-}Bu)_{18}$ cluster. For $Au_{30}S(S\text{-}t\text{-}Bu)_{18}$ cluster, no peak is found at 630 nm, although there are transitions at the same energy because of the same kind of states as in $Au_{30}(S\text{-}t\text{-}Bu)_{18}$. The lower intensity is a result of the size and the aspect ratio change in the gold core induced by the extra, triply coordinated, sulfur atom. As the length of the core is diminished, also the polarization of the induced density is lower which directly affects the absorption intensity. Especially these results show a novel

dx.doi.org/10.1021/ja412141j | J. Am. Chem. Soc. 2014, 136, 5000−5005

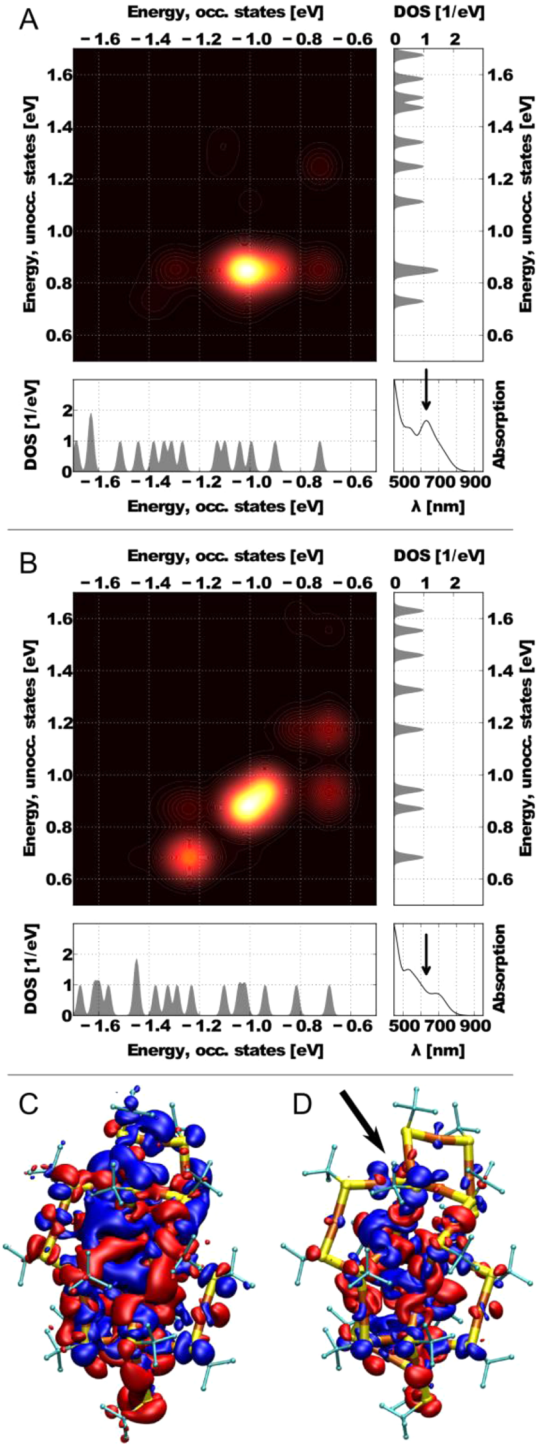

Figure 5. Transition contribution map (TCM) for the 630 nm feature in (A) $Au_{30}(S\text{-}t\text{-}Bu)_{18}$ and (B) $Au_{30}S(S\text{-}t\text{-}Bu)_{18}$. The most intensive transitions are seen from the HOMO−2 state to the LUMO+1 and LUMO+2 states in both of the clusters. The nature of these Kohn−Sham states is consistent between the clusters. Induced densities solved for the feature at 630 nm for (C) $Au_{30}(S\text{-}t\text{-}Bu)_{18}$ and (D) $Au_{30}S(S\text{-}t\text{-}Bu)_{18}$. The positions of the "19th sulphur" is shown by the arrow in (D).

example of a drastic effect on the optical properties of MPCs by only a single (sulfur) atom. The experimental absorption spectra qualitatively confirm the computational observations (Figure 4).

The computed CD spectra of $Au_{30}(S\text{-}t\text{-}Bu)_{18}$ and $Au_{30}S(S\text{-}t\text{-}Bu)_{18}$ are shown in Figure 6. Not surprisingly, the low-energy

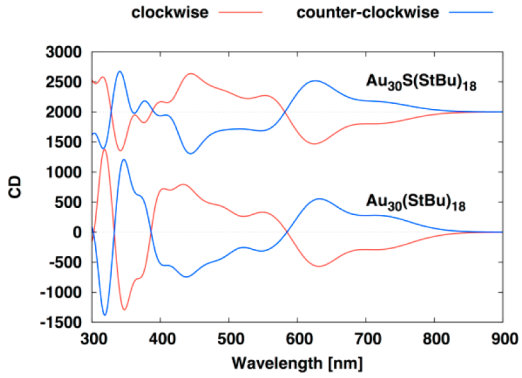

Figure 6. Calculated CD-spectra of $Au_{30}S(S\text{-}t\text{-}Bu)_{18}$ and $Au_{30}(S\text{-}t\text{-}Bu)_{18}$ clusters for both enantiomers based on the crystal structure of $Au_{30}S(S\text{-}t\text{-}Bu)_{18}$.

features above 500 nm are virtually identical to the computed (and measured) spectra of $Au_{28}(SPh\text{-}t\text{-}Bu)_{20}$,[14] since the low-energy features originate from primarily metal-to-metal transitions in the similar chiral cores. When the the spectra of $Au_{30}(S\text{-}t\text{-}Bu)_{18}$ and $Au_{30}S(S\text{-}t\text{-}Bu)_{18}$ are compared, small differences below 450 nm are seen, which are a result of the slight differences in the structure of the gold−thiolate layer discussed above.

Additional Chemical Evidence for the 19th Sulfur. We sought additional support for the presence of the 19th sulfur when compared with the recently reported green gold $Au_{30}(S\text{-}t\text{-}Bu)_{18}$ cluster. For this experiment, it is ideal that one harvests just single crystals solved by XRD experiment, using these to obtain composition using complementary evidence such as mass spectrometry.[16] In practice, it was not possible to collect enough crystals to perform mass spectrometry. We therefore used vials that contained a mixture of single crystals and precipitate for mass spectrometry and optical spectroscopy. ESI-MS in Figure 7 clearly shows the presence of an additional sulfur atom to support $Au_{30}S(S\text{-}t\text{-}Bu)_{18}$ composition determined by XRD. We therefore conclude that $Au_{30}(S\text{-}t\text{-}Bu)_{18}$ is

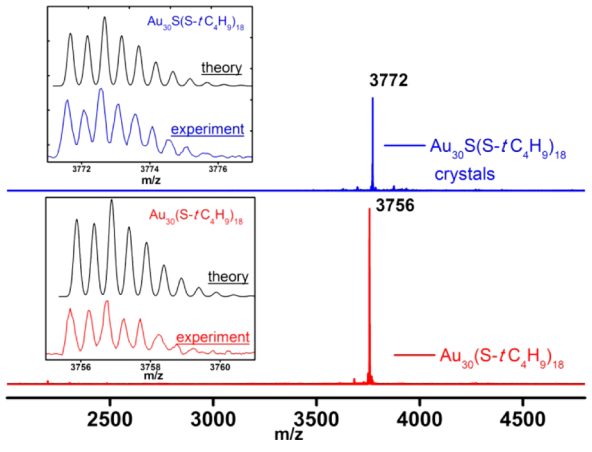

Figure 7. ESI-mass spectra of crystallite particles (blue) and $Au_{30}(S\text{-}t\text{-}Bu)_{18}$ (red). The solution of the crystallite particles clearly support the presence of the 19th sulfur, offering additional chemical evidence for the X-ray structure.

dx.doi.org/10.1021/ja412141j | J. Am. Chem. Soc. 2014, 136, 5000−5005

converted to $Au_{30}S(S\text{-}t\text{-}Bu)_{18}$ during the crystallization process. We also see evidence for a mixture of $Au_{30}(S\text{-}t\text{-}Bu)_{18}$ and $Au_{30}S(S\text{-}t\text{-}Bu)_{18}$ in some other mass spectra not shown here. This could be due either a mixture of crystals and amorphous precipitate or perhaps due to a disordered crystalline system.

Additionally, we solved the X-ray structure on 7 independent samples from various synthetic batches. It is worth noting that the 19th sulfur was present in each crystal. Also, an attempt was made to refine the 19th sulfur position as some other light atom (C, N, O, F, etc.), but the refinement was not successful. On the basis of the extensive mass spectrometry and X-ray diffraction analysis, there is solid evidence for the 19th sulfur and the change from $Au_{30}(S\text{-}t\text{-}Bu)_{18}$ to $Au_{30}S(S\text{-}t\text{-}Bu)_{18}$ upon crystallization.

CONCLUSION

In conclusion, we have resolved experimentally and explained computationally the structural and the optical properties of $Au_{30}S(S\text{-}t\text{-}Bu)_{18}$ and $Au_{30}(S\text{-}t\text{-}Bu)_{18}$ clusters. These clusters show many interesting new features. They have a gold−thiolate protecting layer which consists of a novel triply coordinated sulfur (in case of $Au_{30}S(S\text{-}t\text{-}Bu)_{18}$) and bridging SR-groups, as well as monomeric $Au(SR)_2$ and trimeric $Au_3(SR)_4$ units. We show that the aspect ratio of the core and the optical properties are changed merely by one sulfur atom. We also show important correlations in the chiral nature of $Au_{30}S(S\text{-}t\text{-}Bu)_{18}$ and $Au_{30}(S\text{-}t\text{-}Bu)_{18}$ clusters as compared to the recently resolved $Au_{28}(SPh\text{-}tBu)_{20}$ cluster, also protected by bulky ligands. When these structurally so closely related clusters are now resolved, future studies concentrating on synthesis, growth, and reconstructions of MPC clusters stabilized by bulky thiolates should shed light on fundamental questions regarding our understanding of formation of nanosized gold clusters by thiol wet chemistry.

EXPERIMENTAL SECTION

Materials. 2-Methyl-2-propanethiol (SAFC, ≥99%), 1-adamantanethiol (Fischer, 98%), and *trans*-2-[3(4-tertbutylphenyl)-2-methyl-2-propenylidene]malononitrile (DCTB matrix) (Fluka ≥99%) were purchased from Aldrich. Tetrahydrofuran (destabilized) and other solvents like toluene, methanol, acetonitrile, and acetone were used from Fischer as received. Biorad-SX1 beads (Bio-Rad) were used for the SEC.

Methods. UV−visible absorption spectra were recorded in toluene on a Shimadzu UV-1601 instrument. ESI-MS spectra were acquired on Waters SYNAPT HDMS instrument in HPLC grade THF solvent, without any additives present. The instrument was calibrated using $Au_{38}(SCH_2CH_2Ph)_{24}$ ions, which are closer to the mass of $Au_{30}(SR)_{18}$.

Synthesis, Purification, and Crystallization. Nanoparticles were prepared according to previously published procedure,[6] whereby 0.254 mmol of $HAuCl_4{\cdot}3H_2O$ is dissolved in 15−20 mL of HPLC tetrahydrofuran to which 0.762 mmol of *tert*-butanethiol (2-methyl-2-propanethiol, Acros Organics) is added to give a 1:3 metal−ligand molar ratio. No TOABr was used in the synthesis. After stirring vigorously for 15 min, an aqueous solution of $NaBH_4$ (2.54 mmol, 10x mole ratio) in 10 mL of cold H_2O was added instantaneously. The reaction mixture turned dark in color immediately, and the stirring was continued for 1 h and processed via an initial rotary evaporation of the THF solvent (drying the crude product) followed by sequential rounds of washing with excess methanol and centrifugation to cleanse the product of excess $t\text{-}C_4H_9$. Purification and separation was conducted as reported before,[6] whereby the thermochemical treatment, in a solution of 1:3 (% v/v) toluene/$t\text{-}C_4H_9$ gives rise to >90% pure $Au_{30}(S\text{-}tC_4H_9)_{18}$ after 5 h of stirring at 75 °C. The samples were further purified using size exclusion chromatography (SEC) using HPLC grade THF on Bio-Rad SX1 beads. Crystals were grown by a vapor−vapor diffusion method, whereby the pure product was dissolved in toluene and placed in an ethanol bath. Rhombic plate-like crystals suitable for measurement were obtained within 7−10 days. Single-crystals were confirmed first by a color change of the rhombic plates from a dark brown primary color to a red/scarlet-red secondary color when rotated under the application of plane-polarized light. Crystals were grown from over 20 different synthetic batch products, and formation of crystals was observed more frequently in the title compound than any other system involving $HSCH_2CH_2Ph$ ligand.

Single Crystal X-ray Analysis. Single crystal data collection, structure solution, and refinement were performed on at least 8 independent crystals. Typically, a rhombus shaped crystal was selected under oil under ambient conditions and attached to the tip of a MiTeGen MicroMount. The crystal was mounted in a stream of cold nitrogen and centered in the X-ray beam by using a video camera. The crystal evaluation and data collection were performed on a Bruker APEX II diffractometer with Mo Kα (λ = 0.71073 Å) radiation. The initial cell constants were obtained from three series of ω scans at different starting angles. Each series consisted of 12 frames collected at intervals of 0.5° in a 6° range about ω with the exposure time of 60 s per frame. The reflections were successfully indexed by an automated indexing routine built in the APEXII program suite.

Crystal Data. For $C_{72}H_{162}Au_{30}S_{19}$: triclinic, space group $P\bar{1}$ (no. 2), a = 14.982(5) Å, b = 19.900(7) Å, c = 28.215(10) Å, α = 81.352(7)°, β = 78.546(6)°, γ = 69.930(7)°, V = 7713(5) Å^3, Z = 2, μ(Mo Kα) = 28.681 mm^{-1}, D_{calc} = 3.2492 g/mm^3, 57 513 reflections measured ($1.48 \leq 2\Theta \leq 39.56$), 13 890 unique ($R_{int}$ = 0.0426) which were used in all calculations. Data/constraints/parameters = 13890/216/783. Goodness-of-fit on F^2 = 1.039. The final R_1 was 0.0591 ($I > 2\sigma(I)$) and wR2 was 0.1970 (all data).

Computational Methods. We used the density functional theory (DFT) as implemented in the real-space code-package GPAW (Grid-based Projector-Augmented Wave method).[17,18] Initial structure for DFT-optimization of $Au_{30}(S\text{-}t\text{-}Bu)_{18}$ was obtained from the crystal structure of $Au_{30}S(S\text{-}t\text{-}Bu)_{18}$ by removing the μ_3-S atom. Structure optimization was performed using the local density approximation (LDA) exchange-correlation functional,[19] 0.2 Å grid spacing, and 0.05 eV/Å convergence criterion for the maximum forces acting on atoms in clusters. LDA approximation is known to reproduce the gold−gold distances in the metal core better as compared to the higher-level functionals. The GPAW setups for gold include scalar-relativistic corrections. Optical absorption and circular dichroism spectra were calculated for the LDA relaxed structures using Casida's formulation of the linear response time-dependent DFT[20,21] and PBE (Perdew-Burke-Ernzerhof) functional.[22] Bader charges were calculated using the code provided by the Henkelman group.[23]

ASSOCIATED CONTENT

Supporting Information

Crystallographic information file of $Au_{30}S(S\text{-}t\text{-}Bu)_{18}$; coordinates of the DFT-relaxed $Au_{30}(S\text{-}t\text{-}Bu)_{18}$; table and molecular diagrams. CCDC reference number (cif, fcf, hkl) is 981324. This material is available free of charge via the Internet at http://pubs.acs.org.

AUTHOR INFORMATION

Corresponding Authors

amal@olemiss.edu

hannu.j.hakkinen@jyu.fi

Notes

The authors declare no competing financial interest.

ACKNOWLEDGMENTS

The experimental work was funded by NSF-CHE-1255519 and the theoretical work through the Academy of Finland. The computations were done at the CSC − the Finnish IT Center

for Science. We thank Prof. Nanfeng Zheng for useful discussions and Dr. Ilia A. Guzei for assistance with X-ray structure refinements. S.M. and H.H. thank Kirsi Salorinne for discussions relating to existence of μ_3-S in gold−thiolate complexes.

REFERENCES

(1) (a) Maity, P.; Xie, S.; Yamauchi, M.; Tsukuda, T. *Nanoscale* **2012**, *4*, 4027−4037. (b) Häkkinen, H. *Nat. Chem.* **2012**, *4*, 443. (c) Jadzinsky, P. D.; Calero, G.; Ackerson, C. J.; Bushnell, D. A.; Kornberg, R. D. *Science* **2007**, *318*, 430−433.
(2) Offord, D. A.; John, C. M.; Linford, M. R.; Griffin, J. H. *Langmuir* **1994**, *10*, 883−889.
(3) Dameron, A. A.; Charles, L. F.; Weiss, P. S. *J. Am. Chem. Soc.* **2005**, *127*, 8697−8704.
(4) Krommenhoek, P. J.; Wang, J.; Hentz, N.; Johnston-Peck, A. C.; Kozek, K. A.; Kalyuzhny, G.; Tracy, J. B. *Acs Nano* **2012**, *6*, 4903−4911.
(5) Nishigaki, J.-i.; Tsunoyama, R.; Tsunoyama, H.; Ichikuni, N.; Yamazoe, S.; Negishi, Y.; Ito, M.; Matsuo, T.; Tamao, K.; Tsukuda, T. *J. Am. Chem. Soc.* **2012**, *134*, 14295−14297.
(6) Crasto, D.; Dass, A. *J. Phys. Chem. C* **2013**, *117*, 22094.
(7) Price, R. C. Ph.D. Dissertation, Georgia Institute of Technology, 2006.
(8) Nimmala, P. R.; Dass, A. *J. Am. Chem. Soc.* **2011**, *133*, 9175−9177.
(9) Zeng, C.; Li, T.; Das, A.; Rosi, N. L.; Jin, R. *J. Am. Chem. Soc.* **2013**, *135*, 10011−10013.
(10) Zeng, C.; Qian, H.; Li, T.; Li, G.; Rosi, N. L.; Yoon, B.; Barnett, R. N.; Whetten, R. L.; Landman, U.; Jin, R. *Angew. Chem., Int. Ed.* **2012**, *51*, 13114−13118.
(11) Mednikov, E. G.; Ivanov, S. A.; Dahl, L. F. *Angew. Chem., Int. Ed.* **2003**, *42*, 323−327.
(12) Häkkinen, H.; Walter, M.; Grönbeck, H. *J. Phys. Chem. B* **2006**, *110*, 9927−9931.
(13) Mo, L.-Q.; Jia, J.-H.; Sun, L.-j.; Wang, Q.-M. *Chem. Commun.* **2012**, *48*, 8691−8693.
(14) Knoppe, S.; Malola, S.; Lehtovaara, L.; Bürgi, T.; Häkkinen, H. *J. Phys. Chem. A* **2013**, *117*, 10526−10533.
(15) Yang, H.; Wang, Y.; Huang, H.; Gell, L.; Lehtovaara, L.; Malola, S.; Häkkinen, H.; Zheng, N. *Nat. Commun.* **2013**, *4*, 2422.
(16) Heinecke, C. L.; Ni, T. W.; Malola, S.; Mäkinen, V.; Wong, O. A.; Häkkinen, H.; Ackerson, C. J. *J. Am. Chem. Soc.* **2012**, *134*, 13316−13322.
(17) Mortensen, J. J.; Hansen, L. B.; Jacobsen, K. W. *Phys. Rev. B* **2005**, *71*, 035109.
(18) Enkovaara, J.; Rostgaard, C.; Mortensen, J. J.; Chen, J.; Dulak, M.; Ferrighi, L.; Gavnholt, J.; Glinsvad, C.; Haikola, V.; Hansen, H. A.; Kristoffersen, H. H.; Kuisma, M.; Larsen, A. H.; Lehtovaara, L.; Ljunberg, M.; Lopez-Acevedo, O.; Moses, P. G.; Ojanen, J.; Olsen, T.; Petzold, V.; Romero, N. A.; Stausholm-Moller, J.; Strange, M.; Tritsaris, G. A.; Vanin, M.; Walter, M.; Hammer, B.; Häkkinen, H.; Madsen, G. K. H.; Nieminen, R. M.; Norskov, J. K.; Puska, M.; Rantala, T. T.; Schiotz, J.; Thygesen, K. S.; Jacobsen, K. W. *J. Phys.: Condens. Matter* **2010**, *22*, 253202.
(19) Perdew, J. P.; Wang, Y. *Phys. Rev. B* **1992**, *45*, 13244−13249.
(20) Casida, M. J. C.; Bohr, F.; Guan, J.; Salahub, D. R. In *Recent Advances in Density Functional Methods*; ACS Press: Washington, D.C., 1996; p 145.
(21) Walter, M.; Häkkinen, H.; Lehtovaara, L.; Puska, M.; Enkovaara, J.; Rostgaard, C.; Mortensen, J. J. *J. Chem. Phys.* **2008**, *128*, 244101.
(22) Perdew, J. P.; Burke, K.; Ernzerhof, M. *Phys. Rev. Lett.* **1996**, *77*, 3865−3868.
(23) Tang, W.; Sanville, E.; Henkelman, G. *J. Phys.: Condens. Matter* **2009**, *21*, 084204.